17th World Conference on Earthquake Engineering, 17WCEE
Sendai, Japan - September 13th to 18th 2020

MECHANISM OF STORY COLLAPSE CAUSED BY LOCAL DAMAGE TO REINFORCED CONCRETE FRAME

R. Hasuike[(1)], K. Tajima[(2)], K. Naganuma[(3)]

[(1)] *Master of Eng., Kume Sekkei, Rui.Hasuike@kumesekkei.co.jp*
[(2)] *Associate Professor, Nihon University, tajima.kazuki@nihon-u.ac.jp*
[(3)] *Professor, Nihon University, naganuma.kazuhiro@nihon-u.ac.jp*

Abstract

Column shear failure and the associated story failure resulting from recent large earthquakes have been reported in reinforced concrete (RC) buildings designed according to previous earthquake resistance standards. These failures have been attributed to shortening of columns and roughness of the hoop spacing. At present, the ultimate state of the frame is determined under many assumptions in Japanese seismic diagnosis, because the mechanism of the story collapse has not precisely been elucidated. For this reason, it is important to understand the axial support capacity of a sheared column.

In previous studies, many experiments have been carried out to understand the axial support capacity of a column. However, theoretical analyses and formulations are difficult to carry out because there is a wide range of specimens and complex failure types such as shear failures, and there are few research examples. For example, Elwood et al. theoretically formulated the axial limit curve from a mechanical model focusing on the frictional resistance of the shear crack surface, in order to elucidate the axial failure mechanism after the shear failure of a column. However, only a small number of long columns have been used in that study as the test specimens, and there is insufficient verification of the applicability of the model to short columns. Therefore, in this study, we refer to previous experimental studies on RC columns and create a database that organizes various parameters related to axial failure after shear failure. Based on the experimental database, we propose a modified formula for the axial limit curve that is applicable to a wide range. The feature of this modified formula is that it divides the cases into short columns and long columns. Upon examination of the experimental database, we find a certain linear tendency in the relationship between the effective friction coefficient μ_m of the shear fracture surface and the horizontal deformation at the time of axial failure, and this is because the failure mode and cracking properties have been confirmed to affect the decrease in the effective friction coefficient by a few μ_m.

Finally, with the aim of elucidating the story collapse mechanism of RC frames, we conducted a story collapse simulation using the modified formula. A frame analysis model for a shaking table test of a full-scale 6-story RC frame designed according to previous earthquake resistance standards was constructed. An axial spring was considered, given an axial limit curve that modifies the deterioration of the axial support capacity of a sheared column. The results confirmed that a re-distribution of axial force to adjacent column members is continuously generated, initiating from the deterioration of the axial support capacity of one column, in turn causing a chain of column axial failures that lead to the RC frame finally collapsing.

Keywords: Shear Failure, Axial Failure, Axial Limit Curve, Story Collapse, RC Frame,

© The 17th World Conference on Earthquake Engineering

1. Introduction

In Japan, one of the most earthquake-prone countries in the world, many reinforced concrete (RC) buildings have collapsed or suffered damage from large earthquakes. Cases of RC buildings that suffered shear failure in their columns as well as story collapse when they were struck by large earthquakes in recent years have been reported, especially those designed according to the old earthquake standards prior to 1971. Therefore, many experimental studies of RC column members, designed to elucidate the mechanism of axial failure of columns after a shear failure, have been conducted in Japan [1]~[24]. Furthermore, Elwood et al. studied the phenomenon of axial failure of RC columns after a shear failure and proposed a theoretical relational expression concerning axial forces and collapsing drift angles [25]. However, the number of test specimens used in the verification of the proposed formula is small, and short and long columns, which are typical in Japan, are outside the scope of application of that formula. Moreover, as the mechanism of story collapse of RC frames is yet to be elucidated, the ultimate state of frames in Japanese seismic diagnoses has been determined under many assumptions.

The purpose of this study is to elucidate the story collapse mechanism of RC frames. Hence, we propose modifying the formula proposed by Elwood et al. to extend its application range. Furthermore, we built a frame analysis model with a shaking table test of full-size RC frames and, by incorporating an axial limit curve based on the modified formula into the numerical analysis, we examined the decrease in the axial support capacity of columns that suffered from shear failure. Moreover, we conducted a story collapse simulation of RC frames that focused on the axial force redistribution behavior that was derived from this decrease in the axial support capacity, and we discuss the story collapse mechanism herein.

2. Previously proposed formula

2.1 Shear-friction model

Figure 1 shows the shear-friction model [25]. The balance equation of forces acting on the model is as follows:

$$N \sin\theta = V_{sf} \cos\theta + \frac{A_{st} f_{yt} d_c \tan\theta}{s} \tag{1}$$

$$P = N\cos\theta + V_{sf} \sin\theta + n_{bars} P_s \tag{2}$$

where N: force that acts on the cracked surface vertically (N), θ: critical crack angle (assumed to be approximately 65° from Figure 2), V_{sf}: frictional resistance of the cracked surface (N), s: hoop spacing (mm), A_{st}: sectional area of the hoops (mm^2), f_{yt}; yield strength of the hoops (N/mm^2), d_c: center distance of one pair of hoops (mm), P: axial force (N), n_{bars}: number of bars, P_s: axial force borne by a single bar (N). Moreover, it was assumed that the external shear force V was zero, and the force Vd generated by the dowel action of the main bar was ignored. At this moment, because Vsf is transmitted through the friction on the cracked surface, it can be defined as the following equations using the friction coefficient μ:

$$V_{sf} = N\mu \tag{3}$$

By substituting Equation 3 into Eqs. (1) and (2) and solving the equations simultaneously, the following equation can be obtained:

$$P = \frac{A_{st} f_{yt} d_c}{s} \tan\theta \frac{1 + \mu \tan\theta}{\tan\theta - \mu} + n_{bars} P_s \tag{4}$$

The first term of Equation 4 is the axial load transmitted through shear-friction, and the second term is the axial load transmitted through the main bar. Additionally, Elwood et al. proposed a maximum capacity model that excludes the second term. The effective friction coefficient for this maximum capacity model is given by the following equation:

© The 17th World Conference on Earthquake Engineering

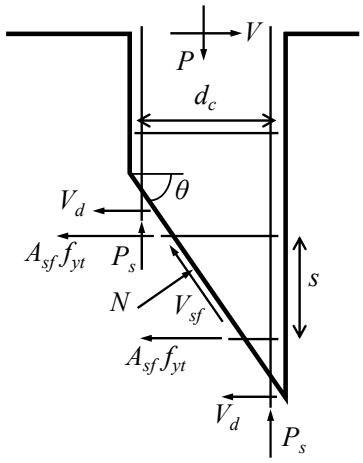

Fig. 1 – Sheat-Friction model

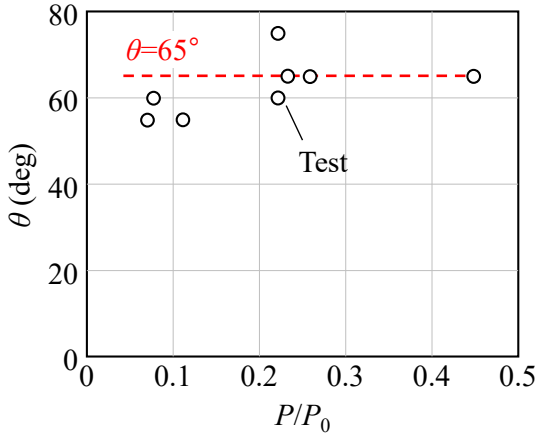

Fig. 2 – Relation between observed angles of critical cracks and axial load

$$\mu_m = \frac{P - \dfrac{A_{st} f_{yt} d_c}{s}}{\dfrac{P}{\tan\theta} + \dfrac{A_{st} f_{yt} d_c}{s} \tan\theta} \tag{5}$$

Based on Equation 5, Elwood et al. calculated the effective friction coefficient for 12 RC column test specimens and derived the equation below, which approximates the relationship between this coefficient and the maximum horizontal displacement observed until the axial failure of the columns:

$$\mu_m = \tan\theta - \frac{100}{4}\frac{\Delta_a}{L} \geq 0 \quad (\theta = 65\,^\circ) \tag{6}$$

This relationship considers the fact that when the horizontal deformation increases, the roughness of the shear-cracked surface deteriorates, thereby decreasing the effective frictional resistance. Finally, by substituting Equation 6 into Equation 4, which contains the second term removed, the following equation can be obtained:

$$\frac{\Delta_a}{L} = \frac{4}{100} \frac{1 + (\tan\theta)^2}{\tan\theta + P\left(\dfrac{s}{A_{st} f_{yt} d_c \tan\theta}\right)} \quad (\theta = 65\,^\circ) \tag{7}$$

Equation 7 (Elwood formula) provides the curve relationship (axial limit curve) between the axial force and drift angle at the moment of axial failure, which exhibited an excellent agreement with the experimental results. However, the number of test specimens used in the verification of the equation was small, and considering that it was verified with a ratio of column height to diameter (h_0/D) higher than 6.4, its applicability to RC short columns, which exhibit a strong tendency to shear failures, was low.

3. Proposal of a modified axial limit curve formula

3.1 Correspondence between previous column experimental database and the Elwood formula

Based on previous RC columns experiments [1] to [25], we created an experimental database for this study. The test specimens used were ones whose axial failure points were defined in the literature as having an acting axial force that could no longer be supported or reached the maximum value when the axial compression was loaded with horizontal displacement applied after horizontal loading; furthermore, the axial failure points reported were defined in the same manner. Table 1 shows the test specimen parameters analyzed. Herein, the

© The 17th World Conference on Earthquake Engineering

columns are classified as short or long depending on whether their h_0/D is larger or smaller than two. A total of 168 columns were examined (93 short columns and 75 long columns), with a reduced scale that ranged between 1/4 and the full size. For the failure mode, the short columns exhibited shear failure, and the long columns axial failure after a shear failure. Moreover, because the long columns were subject to failure due to bending, such as flexural pressure failure, those modes were included in the database for comparison.

Figure 3 shows the comparison between the experimental results collected and the Elwood formula. To calculate the plots of the experimental data, the axial force P obtained from Equation 7 and the values determined from the hoop parameters were set in the vertical axis and the drift angle of the moment of axial failure in the horizontal axis. The graph indicates that in the case of long columns, some of the test specimens agree well with the Elwood formula; however, in general, the axial force at the moment of axial failure is overestimated. Meanwhile, the short columns, exhibit poor correspondence with the Elwood formula; hence, they are out of the application scope.

Table 1 – Test specimen parameters

	Short Column ($h_0/D \leq 2$)	Long Column ($h_0/D > 2$)
h_0/D	1.5~2.0	2.5~6.5
Concrete Strength (N/mm^2)	11.4~35.2	9.4~44.5
Axial Force Ratio $N/(bDf_c)$	0.04~0.89 (1.02*)	0.07~0.99
Yield Strength of Rebar (N/mm^2)	333~502	331~479
Total Reinforcement Ratio (%)	0.16~3.00	0.95~3.13
Yield Strength of Hoop (N/mm^2)	296~425	296~690
Hoop Ratio (%)	0.11~0.68	0.07~1.21

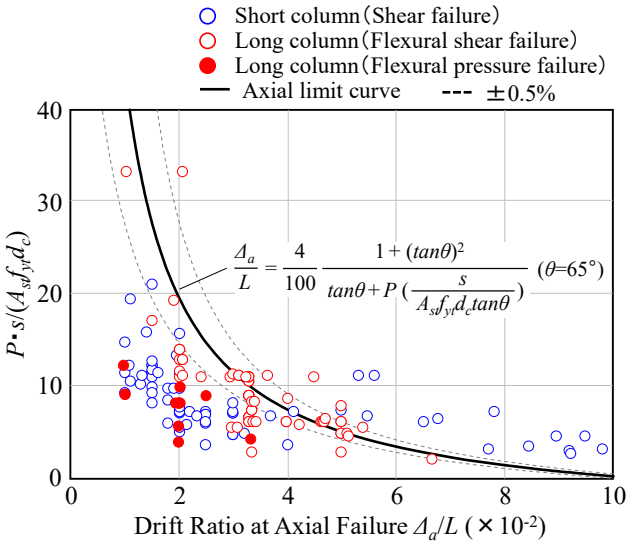

Fig. 3 – Comparison between the experimental results collected and the Elwood formula

3.2 Critical crack angle θ

In the shear-friction model, it is important to set an adequate critical crack angle θ. In this study, to validate the θ = 65° assumed by Elwood et al. from observation results of a few test specimens, based on the experimental database, we measured the shear crack angle from the test specimens whose crack and failure condition could be verified. Figure 4 shows the calculation method of the crack angle and the relationship between the critical crack angle θ and axial force ratio. If a column contains multiple major shear cracks, then the average value of all those cracks is defined as the shear crack angle. The measurement results of all 61 columns are indicated in the graph; however, with the parameters used in this experiment, the results varied around the average of 60.7°, regardless of the axial force ratio or h_0/D. In previous studies [14], the crack angle θ was estimated to be 60°, which is similar to the results of the current study.

3.3 Effective friction coefficient μ_m

When an RC column receives horizontal deformation forces repeatedly, it suffers from damages, such as crushing and peeling of concrete cover and core, in that order. Hence, as implied in Equation 6, as the damage on the shear-cracked surface increases, the effective frictional resistance decreases. However, it is believed that the damage process of the cracked surface varies according to the failure and resistance modes. For example, with the failure mode in the short columns and a large shear resistance component, the damage concentrates on the shear-cracked surface, thereby accelerating its deterioration. Meanwhile, the long columns, which are more susceptible to axial failure after shear failure, have a larger resistance component than that of

© The 17th World Conference on Earthquake Engineering

short columns. Therefore, the damage does not concentrate on the shear-cracked surface; consequently, the deterioration of the cracked surface decelerates. Hence, when determining the linear relationship proposed in Equation 6, the damage progress should be considered. Therefore, the effective friction coefficient, μ_m was estimated based on the experimental database.

Figure 5 shows the relationship between the effective friction coefficient, μ_m and the drift ratio at axial failure, $\Delta a/L$. To determine the plots of the experimental data, the effective friction coefficient, μ_m, was calculated from Equation 5 with $\theta = 60°$. In the short column's case, a linear trend was observed in both areas divided by a drift ratio of approximately 4%. Here, the difference between the two is the number of repetitions of horizontal deformation loading. Data with small deformation are primarily the result of test specimens losing their axial support capacity when the number of repetitions increases gradually. Meanwhile, data with large deformation is the pushover loading or pushover loading after only a few repetitions (two or three). This is likely because the damage progress of the shear cracked surface is affected significantly by the difference in the number of repetitions, causing a significant difference in the degree of decrease in the effective frictional resistance.

In the long column's case, a relatively linear relationship was observed in most parts of the data. However, data that deviate significantly from the linear relationship (marked as out of scope in the graph) were verified. Here, the two plots of data enclosed by a solid line in the graph are the results of the experiment that considered only the number of repetitions as a parameter in the same test specimen [24], and one of them was subjected to 10 repetitions with each deformation. Contrary to the short column case described, in this case, the shear-cracked surface was deteriorated by the high number of repetitions, causing a large difference in the deformation at axial failure despite being the same test specimen. Furthermore, the out-of-scope data enclosed by a dotted line are test specimens with a large axial force ratio (between 0.4 and 0.99). In these specimens,

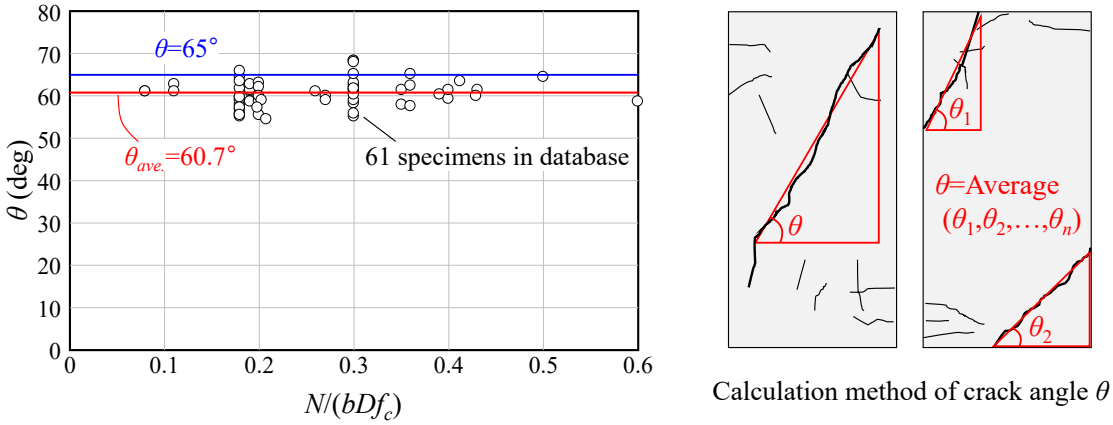

Calculation method of crack angle θ

Fig. 4 –Relation between observed angles of critical cracks and axial load

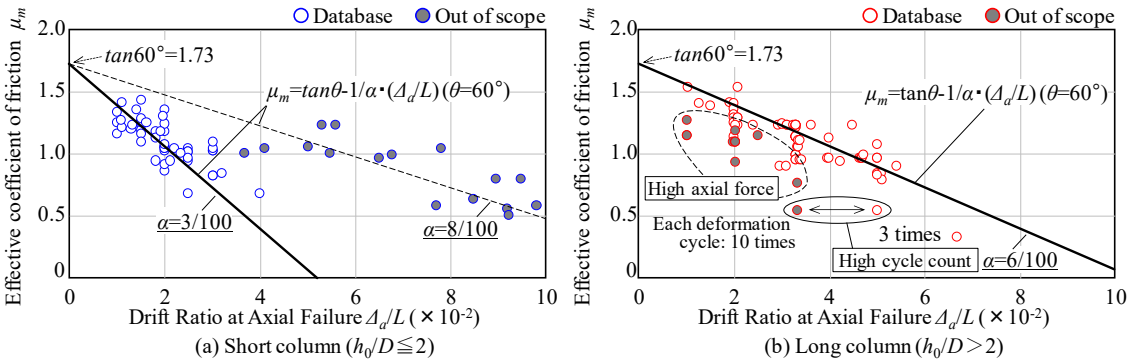

(a) Short column ($h_0/D \leqq 2$) (b) Long column ($h_0/D > 2$)

Fig. 5 – Relation between effective coefficient of friction and the drift ratio at axial failure

© The 17th World Conference on Earthquake Engineering

no formation of shear cracked surface was verified from the failure condition, and the failure mode was of the flexural-pressure type. For these long column specimens, with an axial force ratio that exceeds 0.4, the balance of forces by the shear-friction model cannot be considered; hence, they are excluded in this analysis.

Based on Figure 5, we propose an equation that represents the relationship between the effective friction coefficient, μm and drift angle at axial failure, as follows:

$$\mu_m = \tan\theta - \frac{1}{\alpha}\frac{\Delta_a}{L} \geq 0 \quad (\theta = 60°) \tag{8}$$

$$\alpha = \frac{3}{100} \quad (h_0/D \leq 2) \tag{9}$$

$$\alpha = \frac{6}{100} \quad (h_0/D > 2) \tag{10}$$

The scope of application of this equation is as indicated in Table 1, which is based on the experimental database collected in this study. However, as almost no experiments have been conducted near $h_0/D = 2$, it is necessary to accumulate further experimental data in the future.

3.4 Proposal of a modified axial limit curve formula

Based on the analysis thus far, our proposal for the modified axial limit curve formula initially proposed by Elwood et al. is as follows:

$$\frac{\Delta_a}{L} = \alpha \frac{1+(\tan\theta)^2}{\tan\theta + P\left(\dfrac{s}{A_{st} f_{yt} d_c \tan\theta}\right)} \quad (\theta = 60°) \tag{11}$$

In Equation 11, the numerical value of θ of Equation 7 is changed to 60°, and the coefficient α is newly introduced.

Figure 6 shows the results of the experimental database and the corresponding modified axial limit curve. For comparison, the out-of-scope experimental results and the curves before the modification are included. As shown in Figure 6 (a), the modified formula differs from the Elwood formula in short columns, and the modified formula estimated the experimental results relatively well. Meanwhile, Figure 6 (b) shows almost no difference before and after the modification of the formula in long columns, with both formulas estimating the experimental results adequately. Hence, it can be concluded that the Elwood formula has high applicability for long columns.

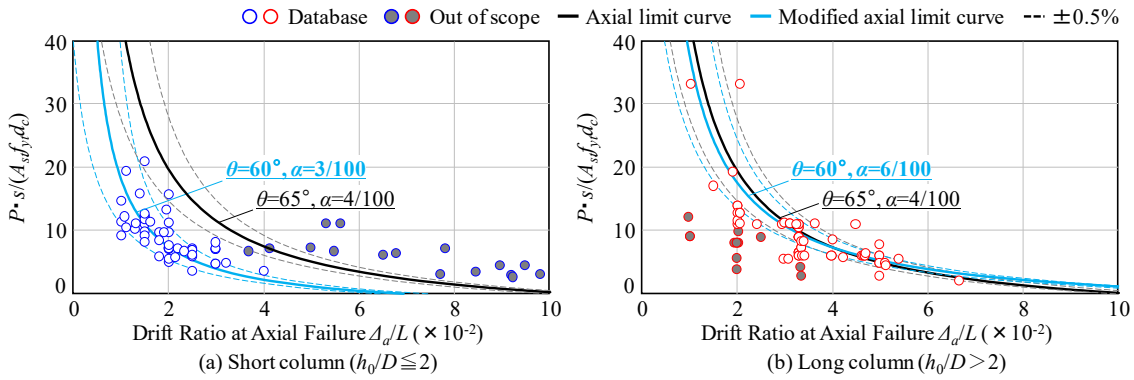

Fig. 6 – Axial capacity model

© The 17th World Conference on Earthquake Engineering

4. Applicability of the modified formula to shear failure behavior of columns

Using the shear limit and axial limit curves proposed by Elwood et al., we previously developed a numerical analysis method capable of expressing the post-peak behavior of RC columns exhibiting shear failure [26]. Using this method, an accurate estimation of the axial failure point of the column members can determine the accuracy of the analysis of yield strength decrease behavior after a shear failure. Therefore, for short columns with $h_0/D \leqq 2$, which exhibited poor applicability of the Elwood formula [13] [14], we conducted a numerical analysis that followed the shear failure behavior of columns. The accuracy of this analysis was verified by comparing the analyses conducted with the axial limit curve before and after the modification.

Table 2 and Figure 7 show the summary of the test specimens analyzed and the analysis model, respectively. The analysis was conducted using OpenSees [27]. The column part of the test specimen was modeled with a fiber element, and a rigid stub was used. Furthermore, to consider the pull-out behavior of the main bar, a joint sub-element was attached to the column head and leg [26]; to consider the shear behavior of the column, a shear sub-element was attached to the column head [26]. The force applied was positive/negative alternating static repetitive loading with a constant axial force applied. Figure 8 shows the material composition rules and the spring restoring force characteristics. The restraint effect proposed by Mander et al. was applied to the core concrete [28]. The iron bar used was a bilinear bar, and the secondary slope after yielding was set to 1/100 the initial rigidity. The restoring force characteristics given to the joint sub-element were modeled with the relationship between moment (M) and angle of rotation (θ) of the bilinear type [26]. The restoring force characteristics of the shear sub-element were determined from the shear crack, shear failure, and axial failure points. The shear deformation of the shear failure point was determined as 25% of the drift angle at shear failure (R = 1/250) [26]. Assuming that the axial failure point reaches axial failure when the shear force is zero, the horizontal deformation at that moment is calculated using Eqs. (7) and (11).

Table 2 –Specifications of specimens

	No.1 [13]	No.3 [13]
$b \times D \times h$	250×250×375	250×250×500
Concrete strength f_c	17.7(N/mm^2)	14.5(N/mm^2)
$N / (b \times D \times f_c)$	0.20	0.21
Longitudinal bar	12-D10	
Hoop	2-D4@55	
yield strength of steel (D10)	353(N/mm^2)	
yield strength of steel (D4)	379(N/mm^2)	

Notation: b=column section width (mm) ; D = column section width depth (mm) ; h = column section height (mm) ; N = axial load (N)

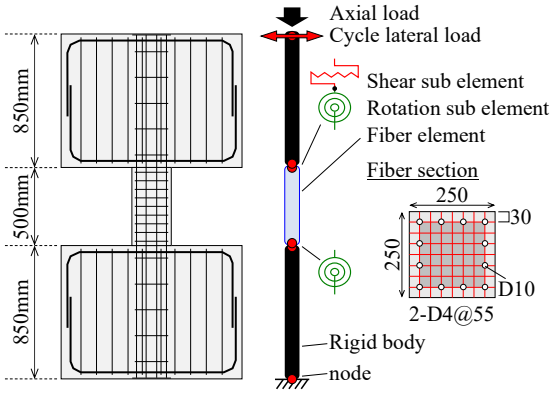

(a) Specimen No.3 (b) Analysis model

Fig.7 – Test specimen and analysis model

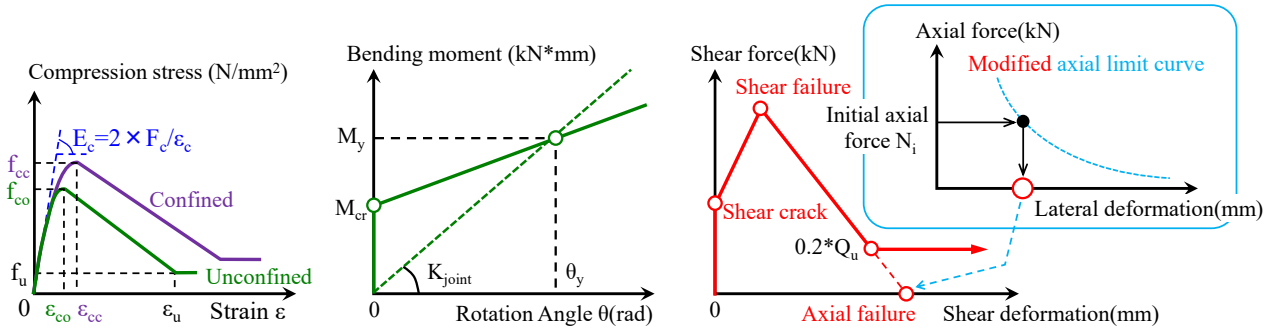

(a) Concrete (b) Sub rotation element (c) Shear sub element

Fig. 8 – Stress-strain relations of material and restroring force characteristics of sub-element

© The 17th World Conference on Earthquake Engineering

Figure 9 shows the axial failure point and axial limit curve of each test specimen before and after the modification. The curves in the graphs represent the relationship between the axial force ratio and member angle with the Elwood and modified formulas. The axial failure points of all test specimens obtained with the modified formula agree well with the experimental results, and the drift angle at axial failure was approximately half that from the Elwood formula.

Figure 10 shows the results of the static repetitive loading analysis with the axial limit curve before and after the modification. In both cases, the analysis and experimental results show a similar behavior until the maximum yield strength is reached. However, in the post-peak area, the analysis results with the Elwood formula showed a gentler yield strength decrease than the experiment because the axial failure point of the shear sub-element shown in Figure 8 was overestimated.

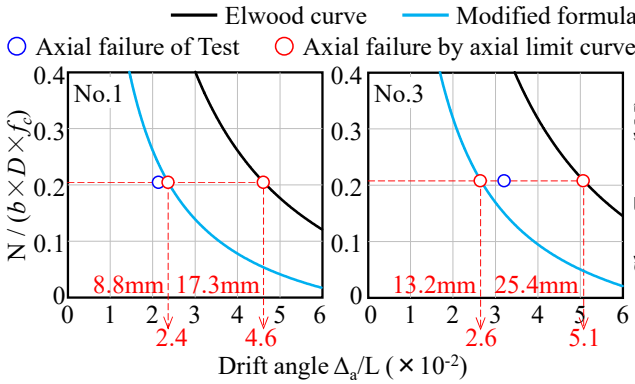

Fig. 9 – Axial failure point

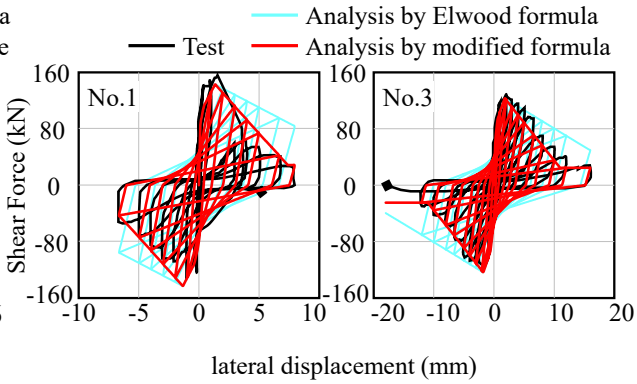

Fig. 10 – Analysis result

5. Story collapse behavior simulation of frames with the modified formula applied

Figure 11 shows the test specimen analyzed. The specimen is a full-size six-story RC frame designed according to the general structural design method of the 1970s, with the columns of one of the exterior planes made short by attaching spandrel walls. Furthermore, the plane of the structure in the middle featured multistory earthquake-resisting walls, but the earthquake-resisting walls of the ground story were removed to form pilotis. The compressive strength of the concrete used was 20 N/mm^2, which is the average value of that era, and the hoop spacing was set to 300 mm.

Figure 12 shows the outline of the analysis model. The column beams are nonlinear elements with fiber cross sections. The spandrel walls were brace substituted by truss elements. The slabs were assumed to be rigid. For the earthquake-resisting and wing walls, the multiple-vertical-line-element model, which is composed of multiple vertical springs and one shear spring [29], was used. Figure 13 shows the restoring force characteristics of the shear spring and axial force decrease spring. The shear failure behavior of the shortened columns was considered by providing a shear sub-element to their head [26]. The axial spring, as with the shear sub-element, was provided to the column heads. The restoring force characteristics were the axial direction and force-axial direction displacement relationship of a single-axis spring; however, its initial condition was rigid. In the analysis, the axial failure point was detected from the positional relationship between the column axial force and axial limit curve, and the maximum axial force of the axial spring was determined. Subsequently, the axial force decreased according to the axial limit curve to reproduce the loss behavior of axial resistance.

To analyze the redistribution behavior of the axial force among the columns of the ground story, a pushover analysis was performed in the Y-direction. By inputting a linearly increasing acceleration with a constant slope, a dynamic pushover analysis was performed, and the amount of time required until the collapse was measured. Considering the stability of the analysis through the calculated load of the axial spring, the slope of linear acceleration was set to a relatively low value, i.e., 1 gal/0.01s. Furthermore, the mass points

© The 17th World Conference on Earthquake Engineering

were arranged as concentrated mass in the center of gravity of each slab. The damping was analyzed as a tangent stiffness-proportional type with a ratio of 3%.

Figure 14 shows the deformation diagram in each event obtained from the analysis. After the column of the ground story exhibited shear failure, the external short columns C2 and C3 and the columns C6 and C7 below the earthquake-resisting wall began to lose axial resistance, and the central part of the frame exhibited axial failure. Consequently, the axial force of the columns around it increased until the entire story collapsed. Figure 15 shows the variation in the column axial force of planes of structure Y1 to Y4 obtained from the analysis. The graphs on the left show the relationship between each column axial force and the sroty drift angle, and the graphs on the right the relationship between time and average change rate of column axial force obtained by differentiating its time history response with time.

The circles in the graphs show the intersection with the axial limit curve (axial failure point); as shown, all columns of the ground story exhibited shear failure, followed by a chain of axial failures until story collapse. From the axial failure flow of the column in the graphs on the left, it is clear that once the axial force of the short column C3 decreases, the adjacent short column, C2, exhibits axial failure continuously. Examining the redistribution tendency of axial force from the graphs on the right, it is clear that the axial force of C3 is redistributed to the column inside the planes of the structure, especially C2. This confirms that the axial support capacity decrease of a single column triggers the redistribution of axial force to the other columns and subsequent axial failure induction as a chain reaction. The simulation showed that this sequence of story collapse behavior occurred from approximately 5.7 s, in as little as 0.1 s, and a complex stress transmission behavior occurred at this time fraction.

Examining more closely at approximately 5.74 s, when the variation is particularly significant, it is clear that after C7 (located below the wall) bears a large variable axial force, an axial failure occurred and the axial resistance is lost rapidly. The largest part of the redistributed axial force at this point is concentrated in C6, located below the adjacent wall. This is likely because the high stiffness ratio of the beams on the wall side

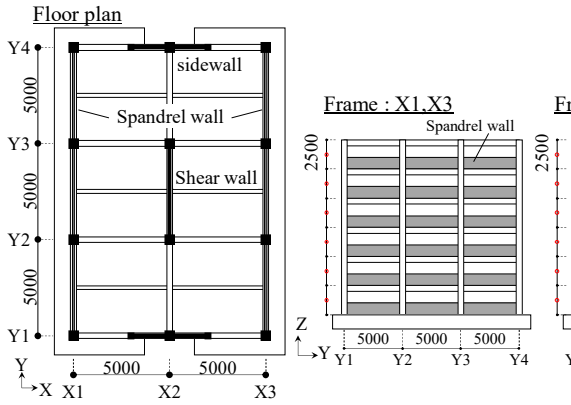

Fig. 11 – Specimen

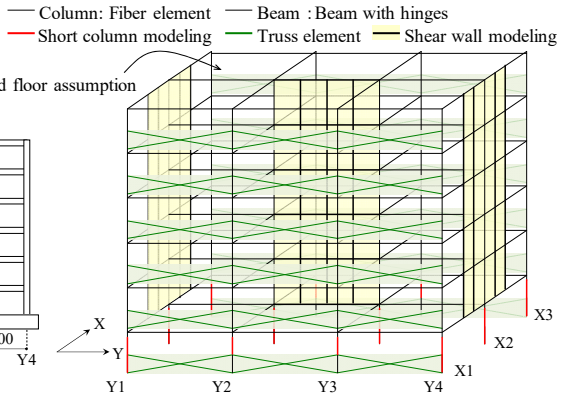

Fig. 12 – Analysis model

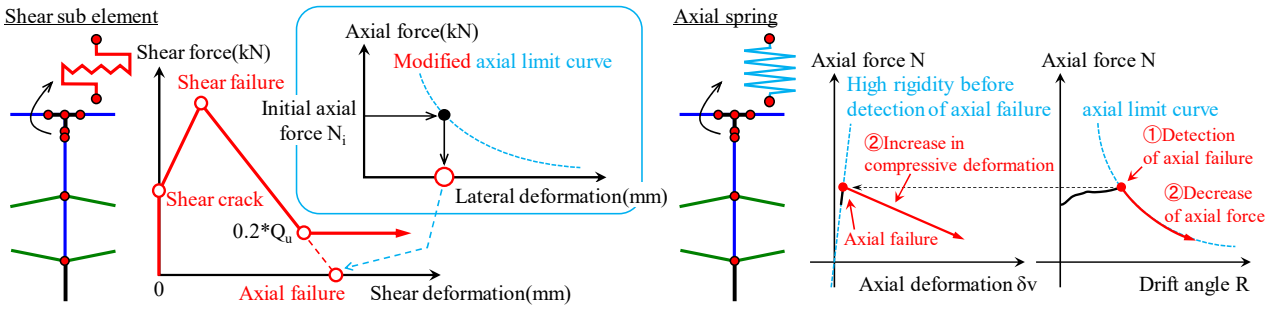

Fig. 13 – Shear sub element and axial spring

© The 17th World Conference on Earthquake Engineering

caused almost the entire axial force to fluctuate between the columns under the wall. Furthermore, in the current seismic diagnosis in Japan, the assessment of type-two structural elements of columns in a piloti frame is based on the assumption that the redistributed axial force is a long-term axial force; however, as indicated by the analysis results, the variable axial force of the columns below the wall is high, which may suggest that the assessment is from the high-risk side.

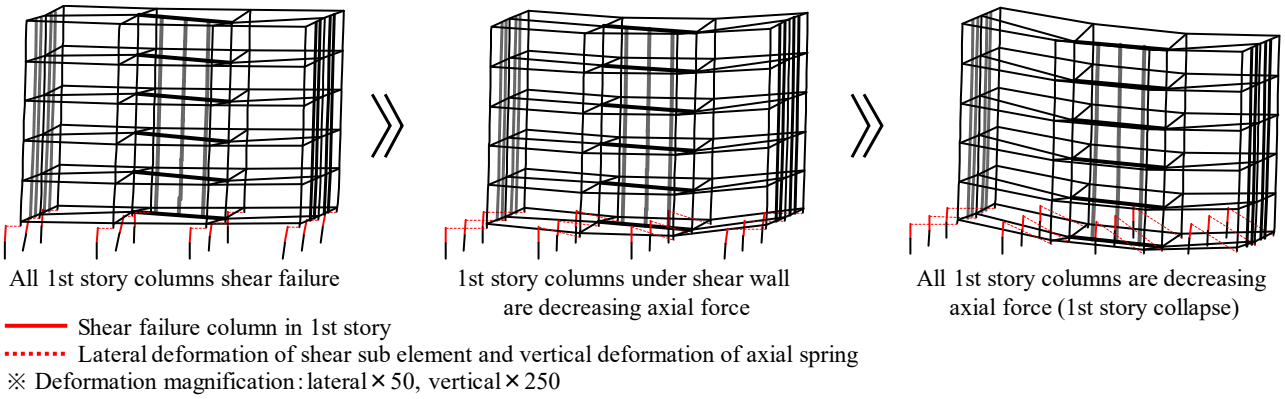

Fig. 14 – Process until 1st story collapse

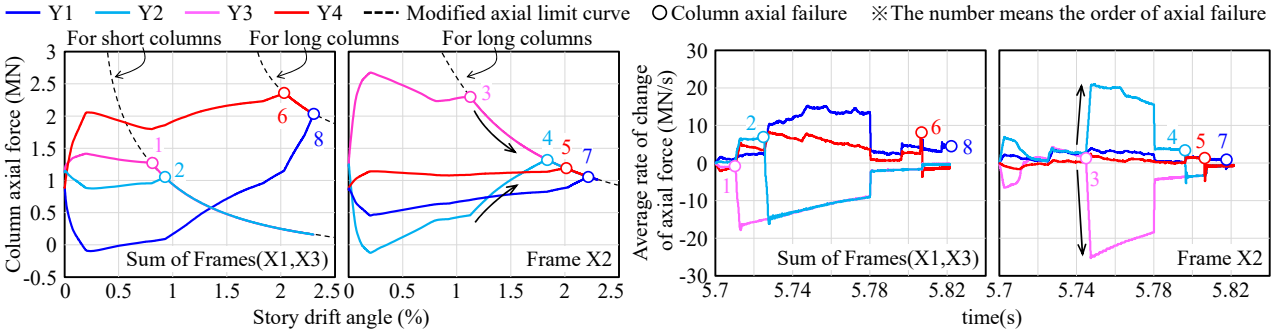

Fig. 15 – Transition of column axial force (Y1 ~ Y4 Frame)

6. Conclusions

The purpose of this study was to extend the scope of application of the axial limit curve formula proposed by Elwood et al. Hence, we proposed a modification to their formula based on a database of previous RC columns member experiments and analyzed the applicability of the modified axial limit curve. The findings obtained are as follows:

(1) The critical crack angle θ in the shear-friction model was defined at 65°; however, based on a re-evaluation of previous experimental results of RC columns, we suggested $\theta = 60°$.

(2) The effective friction coefficient, μm could be determined from the modified formula classified as long and short columns according to the h_0/D value. Additionally, the deterioration of shear-cracked surfaces by repetitive loading could be considered for each failure mode.

(3) The modified formula of the axial limit curve obtained from the proposed critical crack angle θ and the effective friction coefficient, μm estimated the axial failure points of short and long columns adequately. The estimation of short columns, in particular, was more accurate than that of the previously proposed formula, which indicated that the scope of application of the formula was successfully extended.

(4) When the modified formula was applied to a shaking table test of a full-size six-story RC frame, the downward trend of the axial force support capacity of the frame was successfully reproduced. This could be attributed to the effectiveness of the earthquake-resisting walls in preventing a story collapse.

© The 17th World Conference on Earthquake Engineering

(5) The story collapse of the frame started from the decrease in the axial support capacity of a single column, followed by a redistribution of the axial force to the adjacent column members, which induced a chain of axial failures. Furthermore, the axial force applied to the columns to which the axial force was redistributed as a chain was large, suggesting that the assumptions made in the seismic diagnosis may be detrimental.

7. References

[1] Takida I, Nakamura T (2015), Collapse Test of R/C shear Columns with Increasing Axial Load, *Summaries of technical papers of annual meeting Architectural Institute of Japan*, 81-82. (in Japanese)

[2] Takida I, Nakamura T (2014), Collapse Test of Reinforced Concrete Columns subjected to High Axial Load considering Decreased Axial Laod, *Summaries of technical papers of annual meeting Architectural Institute of Japan*, 267-268. (in Japanese)

[3] Nakamura T, Yoshimura M (2014), COLLAPSE TEST OF REINFORCED CONCRETE COLUMNS FAILING IN SHEAR WITH DECREASING AXIAL LOAD, *Transactions of AIJ. Journal of structural and construction engineering*, 79, 701, 987-994. (in Japanese)

[4] Nakamura T (2013), Effects of Decreased Axial Load on Collapse Behavior of Reinforced Concrete Columns, *Summaries of technical papers of annual meeting Architectural Institute of Japan*, 513-514. (in Japanese)

[5] Hirose Y, Kato D (2013), TESTS AND EVALUATING METHOD OF AXIAL LOAD CAPACITY USING COLUMNS WITH LOW CONCRETE STRENGTH, *Journal of structural engineering*. B, 59B, 49-54. (in Japanese)

[6] Nakamura T, Muto S, Ito S, Yoshimura M (2011), Effect of Longitudinal Reinforcement Ratio on Seismic Performance of RC Columns with Shear Mode, *Summaries of technical papers of annual meeting Architectural Institute of Japan*, 161-162. (in Japanese)

[7] Ii H, Hirose Y, Iida H, Kato D (2010), Effects of size and tie bars on axial load carrying capacities of R/C columns failing in shear, *Summaries of technical papers of annual meeting Architectural Institute of Japan*, 199-202. (in Japanese)

[8] Kondo T, Yoshimura M, Nakamura T (2008), Collapse Test of RC Columns by Pseudo-Dynamic Test Method(Part 1~2), *Summaries of technical papers of annual meeting Architectural Institute of Japan*, 553-556. (in Japanese)

[9] Miyajima Y, Abe H, Kato D (2008), Test of axial load capacity of R/C column specimens with various size, *Proceedings of the Japan Concrete Institute*, 30(3), 163-168. (in Japanese)

[10] Abe H, Miyajima Y, Honda Y, Kato D (2008), Test of residual axial load capacity of R/C columns to evaluate effects of reinforcing details, *Proceedings of the Japan Concrete Institute*, 30(3), 1297-1302. (in Japanese)

[11] Murakami E, Masuda Y, Tasai A, Kusunoki K (2008), Experimental study on failure mode of low strength concrete RC column, *Proceedings of the Japan Concrete Institute*, 30(3), 211-216. (in Japanese)

[12] Kato D, Ri Z, Nakamura Y, Honda Y (2007), EXPERIMENTAL STUDY ON RESIDUAL AXIAL LOAD CAPACITY OF R/C COLUMNS, *Transactions of AIJ. Journal of structural and construction engineering*, 619, 127-132. (in Japanese)

[13] Kato D, Ri Z, Nakamura Y, Honda Y (2006), TESTS ON AXIAL LOAD CAPACITY OF SHEAR FAILING R/C COLUMNS CONSIDERING REINFORCING DETAILS, *Transactions of AIJ. Journal of structural and construction engineering*, 610, 153-159. (in Japanese)

[14] Yamazaki K, Tasai A (2006), Study on recommendation for axial load capacity of reinforced concrete columns, *Proceedings of the Japan Concrete Institute*, 28(2), 181-186. (in Japanese)

[15] Ri Z, Kato D (2005), Axial Load Capacity of R/C Columns With Different Reinforcing Defails After Shear Failure, *Summaries of technical papers of annual meeting Architectural Institute of Japan*, 139-140. (in Japanese)

[16] Jin H, Yoshimura M, Nakamura T (2005), Effect of Transverse Walls on Collapse of RC Columns with Shear Mode, *Proceedings of the Japan Concrete Institute*, 27(2), 193-198. (in Japanese)

© The 17th World Conference on Earthquake Engineering

[17] Takaine Y, Yoshimura M, Ishigami S (2004), COLLAPSE OF REINFORCED CONCRETE COLUMNS FAILING IN SHEAR AFTER FLEXURAL YIELDING, *Transactions of AIJ. Journal of structural and construction engineering*, 583, 91-98. (in Japanese)

[18] Takaine Y, Yoshimura M, Nakamura T (2003), COLLAPSE DRIFT OF REINFORCED CONCRETE COLUMNS, *Transactions of AIJ. Journal of structural and construction engineering*, 573, 153-160. (in Japanese)

[19] Nakamura T, Yoshimura M, OWA S (2002), AXIAL LOAD CARRYING CAPACITY OF REINFORCED CONCRETE SHORT COLUMNS WITH SHEAR MODE, *Transactions of AIJ. Journal of structural and construction engineering*, 561, 193-199. (in Japanese)

[20] Talo Y, Nakamura T, Yoshimura M (2001), Axial Load Carrying Capacity of RC Columns Subjected to Seismic Actions, *Proceedings of the Japan Concrete Institute*, 23(3), 217-222. (in Japanese)

[21] Tatematsu N, Ohno Y (2001), Effect of Detail of End of Lateral Reinforcement on Flexural Failure of Reinforced Concrete Columns, *Proceedings of the Japan Concrete Institute*, 23(3), 241-246. (in Japanese)

[22] Mori N, Ohno Y (1999), Influence of detail of end hooks of transverse reinforcement on flexural failure of RC columns, *Summaries of technical papers of annual meeting Architectural Institute of Japan*, 793-794. (in Japanese)

[23] Ohno Y, Miyamoto Y (1998), Effects of Details of End Hooks of Transverse Reinforcement on Structural Performance of Reinforced Concrete Columns, *Proceedings of the Japan Concrete Institute*, 20(3), 493-498. (in Japanese)

[24] Miyamoto Y, Ohno Y, Mori N (1998), Amount of Transverse Reinforcement Required for Ensuring the Ductility of Reinforced Concrete Columns, *AIJ Kinki Chapter research meeting*, 49-52. (in Japanese)

[25] Elwood K. J., Moehle J. P. (2003), Shake Table Tests and Analytical Studies on the Gravity Load Collapse of Reinforced Concrete Frames, PEER-2003/01.

[26] Tajima K, Kawai S, Imai K, Shirai N (2012), Influence of Shear or Flexure-Shear critical RC Column on Seismic Performance of RC Frame, *Proceedings of the Japan Concrete Institute*, 34(2), 337-342. (in Japanese)

[27] Open System for Earthquake Engineering Simulation - Home Page, http://opensees.berkeley.edu/

[28] Mander J. B. (1988), Theoretical Stress-Strain Model for Confined Concrete, *Journal of Structural Engineering*, 114(8), 1804-1826.

[29] Matsumori T, Kabeyasawa T, Shirai K, Katsumata H (2006), Shaking table test on full-scale six-story R/C wall-frame structure, *Proceedings of the Japan Concrete Institute*, 28(2), 409-414. (in Japanese)

[30] Vulcano A, Bertero V, Colotti V (1988), Analytical Modelling of R/C Structual Walls, *Proceedings of 9th WCEE*, 7.

© The 17th World Conference on Earthquake Engineering